

Composite Strategy for Backward-Scattering Reduction of a Wavelength-Scale Cylindrical Object by an Ultrathin Metasurface

Xin-Yao Luo,¹ Wen-Long Guo,^{1,2} Guowen Ding,¹ Mingzhu Du,¹ Ke Chen,^{1,*} Junming Zhao,¹ Tian Jiang,¹ and Yijun Feng^{1,†}

¹*School of Electronic Science and Engineering, Nanjing University, Nanjing, 210093, China*

²*Air and Missile Defense College, Air Force Engineering University, Xi'an 710051, China*

(Received 1 August 2019; revised manuscript received 29 October 2019; published 11 December 2019)

Electromagnetic (EM) cloaks have promising potentials in many real-world applications such as noninvasive detection, EM invisibility, etc. Available methods for concealing large (wavelength scale) objects have still been rarely demonstrated by experiments, especially with sufficient bandwidth and ultrathin cloak thickness. Here, we report a composite strategy for realizing backward-scattering reduction of a wavelength-scale cylindrical target by an ultrathin metasurface. This composite strategy integrates the theories of Mie scattering and microwave network to achieve improved operating bandwidth. As a proof of concept, we experimentally present an ultrathin (0.0156λ , with λ as the working wavelength) conformal metasurface to reduce the backward scattering of a metallic cylindrical object (diameter of 1.217λ) within a frequency band of 7.67%. Further bandwidth improvement is also realized by using two kinds of meta-atoms, working respectively in two neighboring frequency bands and placed in an interleaved form to cover over the cylindrical object. Both simulated and measured results show that more than 10-dB backward-scattering reduction can be obtained within an improved bandwidth of approximately 11.10%. The proposed metasurface encompasses advantages of ultrathin thickness and good performances in backward-scattering reduction, which may open promising perspectives for practical applications such as stealth technique, camouflaging, etc.

DOI: 10.1103/PhysRevApplied.12.064027

I. INTRODUCTION

Over the last decade, electromagnetic (EM) cloaks have attracted long-held attention due to their significance and promising potentials in many practical applications such as low observability, sensing, noninvasive detection, etc [1–5]. By emulating arbitrary EM properties in a desired way, metamaterials and metasurfaces show powerful abilities to manipulate the absorption, scattering, and propagation of EM wave [6–12]. In particular, various metamaterial and metasurface techniques have been explored to achieve EM cloaks by either reducing or diverting the scattering of objects [13–22] spanning from radio-frequency to optical regimes. Among them, cloaks based on transformation optics (TO) [23–26] are a typical category, and considerable research efforts have been devoted to exploring various cloaks [27–32], such as the one-way invisible cloak [29], the first broadband isolated polygonal invisibility cloak for visible light [30], the visible cloaking devices for large-scale objects by using commonly available materials [31], the carpet cloak based on quasiconformal mapping

[32], etc. Such cloaks feature excellent cloaking performances, which usually require specific spatial distributions of rigorous EM parameters that should be realized by bulky metamaterials. As alternative approaches, transmission-line cloaking [33,34] and plasmonic cloaking [35,36] have also spurred many interests due to their well-performed characteristics. Despite the great advances achieved by the above methods, compact, thin thickness and easily implemented EM cloaks are still highly desired especially for advanced and integrated systems.

To this goal, a variety of theoretical approaches have been proposed to reduce the scattering of cloaked objects using various shapes within subwavelength thickness. Mantle cloaks utilizing the concept of scattering cancellation feature extremely thin thickness [37–39], and even possess the capability of concealing a wavelength-scale metallic object by a single-layered metascreen with ultrathin thickness. Such kinds of designs are aimed at reducing the total scattering from the object, which is often accompanied with narrow operating bandwidth and poor performances (the bandwidth of 3-dB scattering reduction is typically less than 6.5%) [40,41].

The pioneering researches mentioned above are focused on actualizing cloaks in an original sense, the core of

*ke.chen@nju.edu.cn

†yjfeng@nju.edu.cn

whose invisible recipe is to minimize the total scattering from the object and render objects invisible irrespective of the direction of observation, the polarization of incoming wave [24,42]. Nevertheless, there are many difficulties to realize a perfect cloak, and in many practical applications, only backward-scattering reduction is needed to achieve monostatic invisibility, making it possible to relieve some of the critical restrictions. Hence, “cloak” used in a stretched sense characterized by its fascinating capability of reducing backward scattering also triggers many interests especially in the microwave regime [43,44]. Recently, another type of ultrathin-cloaking strategy is proposed based on microwave-network theory [2,5,14]. The key step is to construct proper elements that are capable of receiving incoming waves and coupling them into neighboring elements to enable the incident power to flow around the hidden objects, thus efficiently reducing the backward scattering. In order to achieve a thin thickness, the dielectrics filled between the metallic cylinder and the cloak are typically with high permittivity, which brings challenges in fabrication of flexible cloaks for arbitrary metallic objects. Therefore, only numerical simulations are presented for this type of cloak while the experimental demonstration remains a pressing task. Besides, bandwidth-limitation theory has revealed the intrinsic contradiction between operation bandwidth and target size, indicating that an increased dimensionality of the hidden target will bring much greater challenges to cloak design [45,46]. However, in most practical applications, the size of cloaked targets is typically comparable to or even much larger than the wavelength. Hence, it is still highly desirable to experimentally implement an ultrathin EM cloak that can efficiently reduce the backward scattering of objects larger than a wavelength with improved bandwidth.

In this Paper, we propose a composite strategy to actualize an ultrathin microwave conformal metasurface to reduce backward scattering of wavelength-scale metallic cylinders. By judiciously combining the mechanism of mantle cloaking and the concept of microwave network, the proposed composite cloak is conducive to achieving broader operating band on the premise of keeping ultrathin thickness. As an example, we numerically and experimentally demonstrate a conformal metasurface operating

$$P_n^{\text{TM}} = \begin{vmatrix} J_n(k_c a) & Y_n(k_c a) & 0 \\ J_n(k_c a_c) & Y_n(k_c a_c) & J_n(k_0 a_c) \\ J_n(k_c a_c) - j \frac{1}{\eta_c} Z_s J'_n(k_c a_c) & Y_n(k_c a_c) - j \frac{1}{\eta_c} Z_s Y'_n(k_c a_c) & -j \frac{1}{\eta_0} Z_s J'_n(k_0 a_c) \end{vmatrix}, \quad (2)$$

and

$$Q_n^{\text{TM}} = \begin{vmatrix} J_n(k_c a) & Y_n(k_c a) & 0 \\ J_n(k_c a_c) & Y_n(k_c a_c) & Y_n(k_0 a_c) \\ J_n(k_c a_c) - j \frac{1}{\eta_c} Z_s J'_n(k_c a_c) & Y_n(k_c a_c) - j \frac{1}{\eta_c} Z_s Y'_n(k_c a_c) & -j \frac{1}{\eta_0} Z_s Y'_n(k_0 a_c) \end{vmatrix}. \quad (3)$$

around 2.2 GHz, with an ultrathin thickness of 0.0156 wavelength, for reducing the backward scattering of a cylindrical object with diameter of 1.217 wavelength. Moreover, two kinds of meta-atoms with different geometries independently optimized in neighboring bands are combined to successfully extend the relative bandwidth (defined by 10-dB reduction) to about 11.10%. The efficiency of backward-scattering reduction can be well preserved as the cylinder object rotated to different in-plane orientations. The proposed methodology may provide a practical alternative to realize ultrathin cloak operating at low microwave frequencies with improved bandwidth and may exhibit meaningful potentials by the experiments demonstrated in realistic configurations.

II. THEORITICAL ANALYSIS

A. Design of mantle cloak

Considering a simple case that a metallic cylinder object with wavelength-scale radius a is covered by an ultrathin metasurface to form a cloaked cylinder with radius a_c , as illustrated in Fig. 1. Since the constituent meta-atom of the patterned metasurface has subwavelength-scaled dimensionalities, the metasurface can be characterized as a homogeneous surface with averaged surface impedance of $Z_s = R_s + jX_s$. This surface impedance can relate the induced averaged electric current density \mathbf{J}_s to the tangential electric field on the surface (averaged over the surface of meta-atom) as $\mathbf{E}_t = Z_s \mathbf{J}_s$, in which $\mathbf{J}_s = \hat{n} \times (\mathbf{H}_t^{\text{out}} - \mathbf{H}_t^{\text{in}})$, and $\mathbf{H}_t^{\text{out}}$ and \mathbf{H}_t^{in} are the tangential magnetic field in the outer and inner sides of the patterned metasurface, respectively. For simplicity, we assume that the metasurface is lossless, in which the equivalent surface impedance Z_s is purely imaginary.

When the object is illuminated by a monochromatic transverse-magnetic (TM) plane wave, the solution of Mie-scattering coefficients c_n^{TM} from the cloaked object can be obtained as [37–40]

$$c_n^{\text{TM}} = -\frac{P_n^{\text{TM}}}{P_n^{\text{TM}} - jQ_n^{\text{TM}}}, \quad (1)$$

where P_n^{TM} and Q_n^{TM} are given by

$$\begin{aligned} P_n^{\text{TM}} &= \begin{vmatrix} J_n(k_c a) & Y_n(k_c a) & 0 \\ J_n(k_c a_c) & Y_n(k_c a_c) & J_n(k_0 a_c) \\ J_n(k_c a_c) - j \frac{1}{\eta_c} Z_s J'_n(k_c a_c) & Y_n(k_c a_c) - j \frac{1}{\eta_c} Z_s Y'_n(k_c a_c) & -j \frac{1}{\eta_0} Z_s J'_n(k_0 a_c) \end{vmatrix}, \\ Q_n^{\text{TM}} &= \begin{vmatrix} J_n(k_c a) & Y_n(k_c a) & 0 \\ J_n(k_c a_c) & Y_n(k_c a_c) & Y_n(k_0 a_c) \\ J_n(k_c a_c) - j \frac{1}{\eta_c} Z_s J'_n(k_c a_c) & Y_n(k_c a_c) - j \frac{1}{\eta_c} Z_s Y'_n(k_c a_c) & -j \frac{1}{\eta_0} Z_s Y'_n(k_0 a_c) \end{vmatrix}. \end{aligned} \quad (2)$$

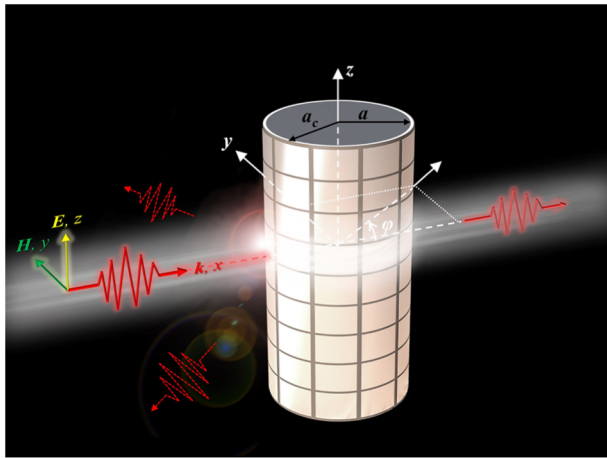


FIG. 1. Schematic of the metallic cylinder covered by a meta-surface cloak composed of patch-shaped meta-atoms.

Here, $J_n(x)$ and $Y_n(x)$ are the n th Bessel and Neumann function, respectively. The parameters k_c and η_c represent the wave number and wave impedance in the region between the metallic cylinder and the patterned surface, while k_0 and η_0 are the ones outside the cloak.

For wavelength-scale cylinders, high-order scattering coefficients will increase. Therefore, we should minimize the total scattering coefficients of $|c_0^{\text{TM}}|^2 + |c_1^{\text{TM}}|^2 + |c_2^{\text{TM}}|^2 + \dots$ rather than forcing only $|c_0^{\text{TM}}|^2 = 0$ as conventionally do for electrically small object [20]. As an example, we consider a metallic cylinder with diameter $2a = 166$ mm (1.245 wavelength at 2.25 GHz) and a height of $H = 324$ mm. This metallic cylinder is covered by a homogeneous, dispersionless, and lossless dielectric layer with thickness of $t = a_c - a = 2.33$ mm (0.017 wavelength at 2.25 GHz) and permittivity of $\epsilon_r = 3.0$. The calculated square of the normalized amplitudes of Mie-scattering coefficients $|c_n^{\text{TM}}|^2$ at several discrete frequencies within the band of interest is depicted in Fig. 2(a). Although $|c_0^{\text{TM}}|^2$ contributes a lot to the total scattering, it is no longer the only dominating term for the case of metallic cylinder larger than a wavelength ($2a \geq \lambda$), and instead, the

first, third, fourth, and fifth multipoles collectively make significant contributions to the total scattering at these frequencies. It should be noted that all the terms are normalized to $|c_0^{\text{TM}}|$. We do not consider n larger than 12, because the magnitude vanishes for $n > 12$ as the figure indicates, thus the reasonable large range of n will not affect the accuracy of the analytical results.

The ideal cloaking effect requires that all the scattering from the object should be well suppressed to result in a zero scattering, making the object perfectly invisible. To this end, Eq. (2) should be zero to ensure a zero total scattering [or Eq. (1) approaches zero]. As indicated in Eq. (1), for a given cylinder and working wavelength, the surface impedance Z_s will be the only degree of freedom for controlling the scattering. By setting $P_n^{\text{TM}} = 0$ in Eq. (2), we can derive the explicit form of the required surface impedance (Z_{sn}) for nullifying each order of the scattering terms, and thus minimizing the total scattering. The required surface impedance is written as [40]

$$Z_{sn} = -\frac{j}{\frac{1}{\eta_c} \frac{J_n(k_c a) Y'_n(k_c a_c) - J'_n(k_c a_c) Y_n(k_c a)}{J_n(k_c a) Y_n(k_c a_c) - J_n(k_c a_c) Y_n(k_c a)} - \frac{1}{\eta_0} \frac{J'_n(k_0 a_c)}{J_n(k_0 a_c)}}. \quad (4)$$

Therefore, by solving Eq. (4), we can calculate the required surface reactance to suppress dominant Mie-scattering coefficients, as shown in Fig. 2(b). Interestingly, the required surface reactances (X_{s0} , X_{s2} , X_{s3} , and X_{s4}) are close to each other, offering us an opportunity to simultaneously suppress all the dominant scattering multipoles ($|c_0^{\text{TM}}|^2$, $|c_2^{\text{TM}}|^2$, $|c_3^{\text{TM}}|^2$, and $|c_4^{\text{TM}}|^2$) with a single layer of metasurface. To this goal, the metasurface should have a surface reactance around -40Ω at 2.25 GHz, as observed from Fig. 2(b). Then, we substitute several surface reactances around -40Ω into Eq. (1) to find the optimal result. It concludes that the metasurface should have a surface reactance of $X_s = -42.5 \Omega$ for the sake of minimizing $\sum_{n=0}^{N_{\max}} |c_n^{\text{TM}}|^2$ at 2.25 GHz, and details can be found in the Supplemental Material [47].

Previous metasurface techniques have suggested various geometries for realizing desired surface reactance [48].

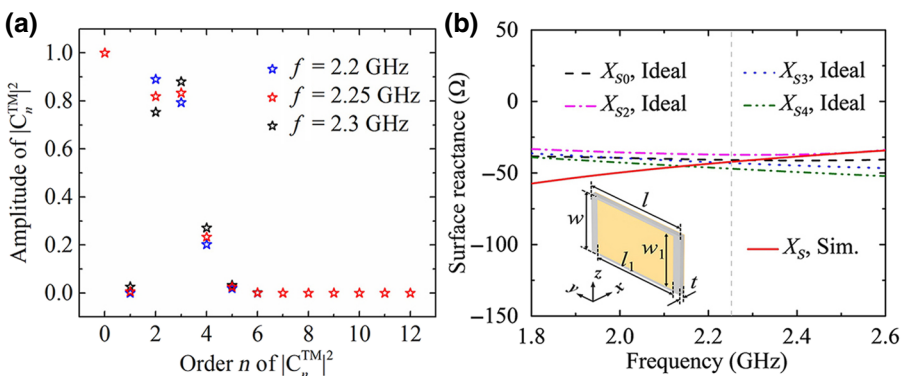


FIG. 2. (a) $|c_n^{\text{TM}}|^2$ for different scattering orders when the cylinder is illuminated by TM-polarized plane wave at normal incidence at several frequencies. (b) The extracted surface reactance of the patch-shaped meta-atom and the analytically calculated ones (ideal ones) required to minimize the dominant scattering terms for the metallic cylinder shown in Fig. 1 ($2a = 166$ mm, $2a_c = 170.66$ mm). Inset shows the schematic of the planar meta-atom.

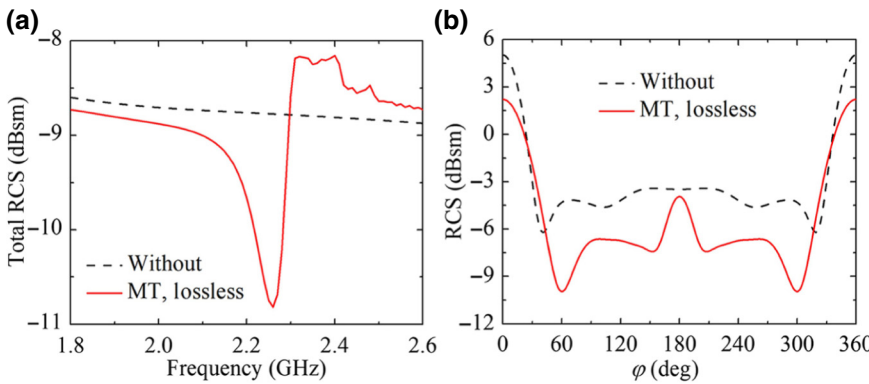


FIG. 3. Simulated (a) total RCS and (b) azimuthal scattering pattern (x - o - y plane) of the metallic cylinder with and without the cloak designed by Mie theory (MT for short).

Here, we choose the patch array as an example to form the metasurface, due to its simplicity in structure configuration, flexibility of design, and potential in broadband performance. The planar form of constituent meta-atom is shown in the inset of Fig. 2(b). By solving the transmission line model (detailed in the Supplemental Material [47]) of the meta-atom, the surface impedance of the single-layered patch can be calculated by [3,10,49,50]

$$Z_s = \frac{j Z_0}{\tan[\phi_r(f)/2] - \sqrt{\epsilon_r} \cot\left(\frac{2\pi}{\lambda_r} t\right)}, \quad (5)$$

where Z_0 is the wave impedance in free space, λ_r is the wavelength in the dielectric spacer, and $\phi_r(f)$ is the phase of the reflection coefficient computed by full-wave simulation software (the CST MICROWAVE STUDIO) at the surface of the meta-atom. By adjusting the geometries of patch pattern, the reflection phase can be controlled as well, offering flexible tuning of the surface impedance. Then, by periodically extending the patches in the metasurface to wrap the cylinder, such conformal metasurface can be approximately viewed as a homogenous impedance sheet acting as the required cloak. The optimal physical parameters to achieve a surface reactance of $X_s = -42.25 \Omega$ are $l = 53.4$ mm, $w = 36$ mm, $l_1 = 48$ mm, and $w_1 = 33.4$ mm. The surface reactance of the metasurface as a function of frequency is shown in Fig. 2(b), where the designed surface reactance intersects with the ideal surface reactance required to minimize each dominant scattering term around the designed frequency of 2.25 GHz.

To evaluate the cloaking performances, we extend the patch-shaped meta-atoms to cover the metallic cylinder, as shown in Fig. 1. Then, we calculate the far-field scattering pattern of the metallic cylinder covered with and without conformal metasurface in CST Microwave Studio using a time-domain solver. The cylinder object is illuminated by a TM-polarized plane wave at normal incidence, with open boundary conditions applied to three orthogonal directions to mimic the free-space environment. In Fig. 3(a), we plot the simulated total radar cross section (RCS) of the metallic cylinder with and without cloak. A

suppression of total scattering is observed for the cloaked cylinder around the design frequency of 2.25 GHz but with a limited bandwidth and efficiency. The difficulty of simultaneously nullifying all dominant scattering terms for such a wavelength-scale cylinder at a certain frequency by single-layered metasurface results in the nonideal scattering reduction of the designed cloak, which is inevitable due to the limited degrees of freedom. Although our analytical model have not considered the curvature effects in the realistic model, the reasonably subwavelength-scaled dimensions of the meta-atom can ensure a negligible shift of the working band between meta-atom design and the whole cloak [48].

To give further insights into the scattering performance of the cloak, Fig. 3(b) illustrates the simulated scattering pattern (x - o - y plane) of the metallic cylinder with and without cloak at the frequency of 2.25 GHz. Compared with the bare cylinder, good suppression effect of scattering is observed for the cloaked cylinder nearly in all azimuthal directions. Nevertheless, the reducing effect of backward scattering ($\phi = 180^\circ$) is quite limited, leading to a poor monostatic RCS performance.

Actually, tremendous practical applications require low backward scatterings, e.g., stealth technique to escape from detection. Considering this, we focus on the performance of monostatic (backward) RCS reduction in what follows, and propose a composite strategy to extend the operating bandwidth. We attempt to introduce the concept of microwave network and investigate the possibility of backward-scattering reduction by guiding incident EM wave to flow around the object's surface at a neighboring frequency, in addition to the existing performance of the mantle cloak around 2.25 GHz.

B. Composite strategy for expanding bandwidth

The key point of the composite strategy is to guide the incident wave to flow around the cylindrical object without affecting the characteristics of the abovementioned mantle cloak. With this in mind, the meta-atoms should be capable of efficiently transferring incident wave to the neighboring

elements, finally forming a microwave network to reduce the backward scattering [2]. Besides, the meta-atoms, as the building blocks to construct the microwave transmission network, are expected to resonant in the neighboring frequency band with respect to the predesigned mantle cloak to form continuously expanded bandwidth.

As a practical structure, microstrip lines are frequently used to confine the wave within the structure and efficiently guide the wave along a well-defined route between two connecting devices. Based on this consideration, we connect the patch structures shown in Fig. 2(b) with microstrip lines to guide the incident wave flowing from one meta-atom to the neighboring one. In this way, a new meta-atom is formed and can be treated as the building block to form the equivalent microwave transmission network, as depicted in the inset of Fig. 4(a). The physical parameters of the microstrip line are $d_1 = 18$ mm and $w_2 = 0.8$ mm. To evaluate the wave energy coupled from one element to its adjacent counterpart, we implement a simulation of the element with open (add space) boundary condition in all directions. Exciting the meta-atom with port 1 and 2, depicted in the inset of Fig. 4(a), a transmission window is observed around 2.15 GHz from Fig. 4(a), in which the transmission reaches its peak while the reflection drops to a dip, showing the possibility of coupling wave energy between neighboring meta-atoms around 2.15 GHz.

The meta-atom in the inset of Fig. 4(a) is capable of coupling the incident wave and transferring it to the neighboring meta-atom at 2.15 GHz. Ideally, this EM behavior should not influence the working state of the mantle cloak designed around 2.25 GHz. Hence, we turn to verify whether its surface reactance can still achieve a minimized scattering coefficient of $\sum_{n=0}^{N_{\max}} |c_n^{\text{TM}}|^2$ at 2.25 GHz. We extract the effective surface reactance of the meta-atom for normal incidence by Eq. (5), and Fig. 4(b) shows the surface reactance in the frequency band of interest. It is demonstrated that a surface reactance of $X_s = -42.25 \Omega$ can still be obtained around 2.25 GHz, indicating that the newly added microstrip lines have little effect on the predesigned mantle cloak. Therefore, this meta-atom can operate as either a mantle cloak at 2.25 GHz or a microwave transmission

network at 2.15 GHz, both of which can be employed to reduce backward scattering of a cylindrical object. This observation motivates us to use the composite strategy that combines both mechanisms of Mie-scattering theory and microwave transmission network for the sake of expanding the bandwidth of monostatic RCS suppression.

III. METASURFACE CLOAK BASED ON THE COMPOSITE STRATEGY

To validate the proposed composite strategy, a conformal metasurface is formed. Considering the influence of the curvature effect of the cylinder, we conduct a careful optimization of the conformal metasurface with slight change of the structure configuration. Herein, optimizations are implemented in CST Microwave Studio and the goal is set as efficient backward-scattering suppression of metallic cylinder with a bandwidth as wide as possible. The optimized meta-atom is shown in the inset of Fig. 5(a), and more details can be found in Supplemental Material [47].

Simulated with open (add space) boundary conditions in all directions, the metallic cylinder (diameter of 166 mm or 1.217 wavelength) covered by the designed metasurface exhibits strong suppression of backward scattering, especially at frequencies of 2.15 GHz (reduced by -15.57 dBsm) and 2.25 GHz (reduced by -19.34 dBsm), as demonstrated in Fig. 5(a). Within the band of 2.15–2.25 GHz, backward scattering can be well suppressed at least by 10 dB. Furthermore, total RCS performances of the bare and covered cylinders are also shown in Fig. 5(b). Compared with the counterpart in Fig. 3(a), the results shown in Fig. 5(b) can achieve a broader bandwidth of the total RCS suppression. This is due to the fact that the mechanisms of both the mantle cloak and microwave transmission network do contribute to total RCS reduction [2,20,37]. We also provide the electric field and power flow distributions for different scenarios in the Supplemental Material [47] to give a more intuitive viewing of the proposed composite strategy, and we find that the microwave transmission network contributes more to the reduction of backward scattering.

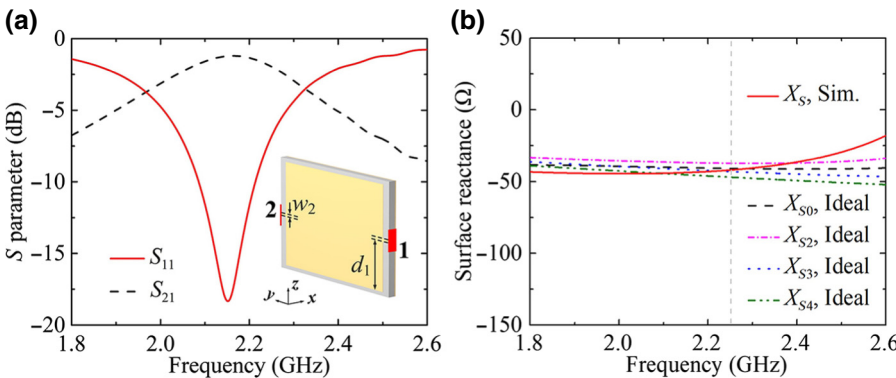


FIG. 4. (a) S_{11} and S_{21} of the planar meta-atom (shown in the inset) for the equivalent microwave transmission network. (b) The extracted surface reactance and the required ones (ideal ones) calculated by Mie-scattering theory.

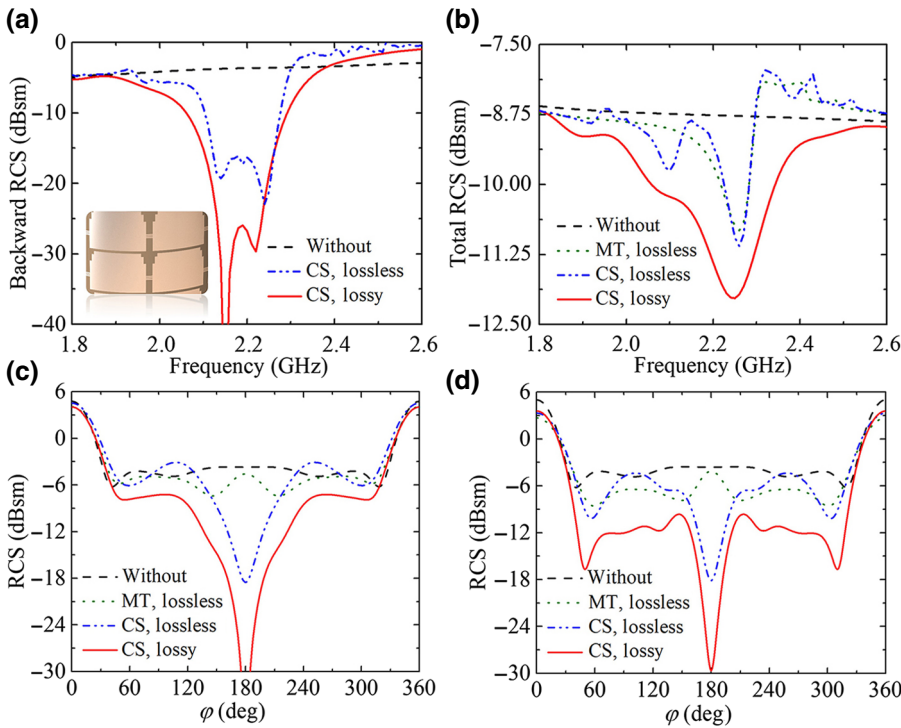


FIG. 5. Simulated (a) backward and (b) total RCS comparisons for different scenarios, and the corresponding simulated RCS in x - o - y plane at (c) 2.15 GHz and (d) 2.22 GHz. (CS or MT represents composite strategy or Mie theory, respectively.) Enlarged view shows the constituent meta-atoms of the metasurface cloak designed by the proposed composite strategy.

In the above, we discuss the composite strategy for designing conformal cloak with lossless materials. However, normal materials including dielectric and metal intrinsically have loss that cannot be neglected during the design process. Actually, the lossy components may also bring useful absorptions, which is conducive to the backward-scattering reduction, providing possibilities to further extend the operation bandwidth [44,51]. Considering these, we divide the ultrathin dielectric layer into two layers, as depicted in Fig. S2(b) of the Supplemental Material [47]. Taconic TSM-DS3 is chosen as the outer dielectric layer [brown layer shown in Fig. S2(b)], which has permittivity $\epsilon_{r1} = 3.0$ with loss tangent $\tan(\delta_1) = 0.0011$ and thickness of 0.13 mm. FR4 dielectric with permittivity $\epsilon_{r2} = 3.0$, $\tan(\delta_2) = 0.041$ and thickness of 2.2 mm is chosen as the inner dielectric layer [white layer shown in Fig. S2(b)]. Consequently, the results for the backward-scattering reduction of such a realistic scenario indeed enhances the bandwidth compared with the lossless ones, as verified in Fig. 5(a). It can be seen that the backward scattering is further suppressed, especially at 2.15 and 2.22 GHz (-52.56 dBsm and -26.05 dBsm, respectively), despite a little deviation of the working frequency of the mantle cloak. This deviation may be induced by the lossy substrates that introduce the real part to the surface impedance, which perturbs the predesigned surface impedance of the mantle cloak. Accordingly, the total RCS of the realistic scenario can be further suppressed, as presented in Fig. 5(b). The detailed influences of the dielectric loss and the real part of surface impedance on the

backward-scattering reduction can be found in the Supplemental Material [47], and we find that the introduction of the lossy component is beneficial for the improvement of backward-scattering reduction.

To give a physical insight into the working mechanism of composite strategy, the simulated far-field RCS patterns on the cut of x - o - y plane (as shown in Fig. 1) at 2.15 and 2.22 GHz are investigated in Figs. 5(c) and 5(d). Compared with the lossless cloak purely designed by Mie-scattering theory, the optimized one using composite strategy is found to achieve remarkable reduction of backward scattering at both frequencies. For the lossy case, the monostatic RCS ($\varphi = 180^\circ$) of the cloaked object can be further decreased due to the existence of EM absorption.

To further validate the composite strategy for backward-scattering reduction, the metasurface fabricated by the standard printed-circuit-board (PCB) technique is wrapped onto an aluminum cylinder, as depicted in Fig. 6(a). We experimentally measure it in a microwave anechoic chamber to avoid unwanted interferences from surroundings. A pair of horn antennas is laid symmetrically about x - o - z plane to measure the backward RCS (see Supplemental Material [47]). We compare the absolute backward RCS of the metallic cylinder with and without conformal metasurface in Fig. 6(b). The measured bandwidth defined by 10 dB (or 10-dB backward RCS reduction bandwidth) can range from 2.119 to 2.288 GHz, around 7.67% fractional bandwidth with respect to the center frequency of 2.20 GHz. Clearly, good coincidence can be observed between the measurement and simulation results in spite

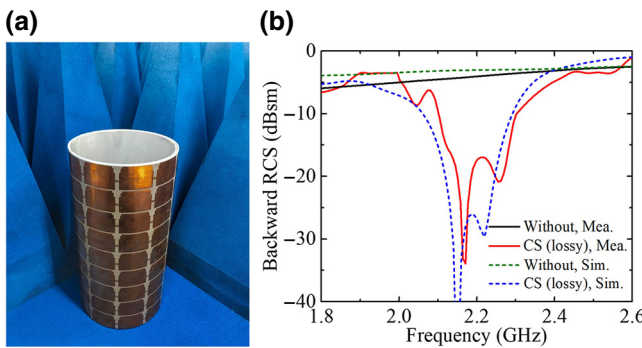


FIG. 6. (a) Photograph of the fabricated prototype. (b) Simulated and measured backward RCS results of the cylindrical object with and without metasurface cloak.

of a little frequency shift that may be caused by fabrication errors of the sample's thickness.

IV. BANDWIDTH ENHANCEMENT FOR RCS REDUCTION

In the above sections, we actualize bandwidth-enhanced backward-scattering reduction by employing the proposed composite strategy. However, it is still challenging and desirable if the bandwidth can be further expanded so that it may be more favorable in real-world applications. Here, we attempt to introduce a well-performed method to improve the bandwidth of the proposed cloak. The key steps of the designing method include first, optimizing two meta-atoms operating in two neighboring frequency

bands according to the composite strategy; then, alternately arranging them one by one to form the whole cloak, as schematically shown in Fig. S8 of the Supplemental Material [47]. Here, Taconic TSM-DS3 with a thickness of 0.13 mm is used as the outer dielectric layer and the polyvinyl chloride (PVC) with relative permittivity $\epsilon_r = 2.6 - 0.015j$ and thickness of 2.0 mm is used as the inner dielectric layer. Through careful optimization, two meta-atoms, denoted by unit A and unit B as shown in the inset of Fig. 7(a), are designed to work in two neighboring bands according to the proposed composite strategy (details of the two meta-atoms can be found in Supplemental Material [47]).

The schematic of conformal metasurface composed of a 10×10 array of pure unit As is plotted in Fig. S8(a) of the Supplemental Material [47], and its result of backward-scattering reduction is depicted by the blue line in Fig. 7(a), which has moderate bandwidth with two reduction dips at 2.23 and 2.42 GHz. It can be seen that the two bands are separated by a scattering peak (pole), and both of the two working bandwidths are below 5%. Similarly, the metasurface cloak implemented by bare unit Bs is illustrated in Fig. S8(b) of the Supplemental Material [47]. The green line in Fig. 7(a) presents its capability of suppressing the backward scattering, showing two backward-scattering dips at 2.26 and 2.36 GHz as well as a total bandwidth of 7.84%. The two parallel slots etched from the top metallic pattern of meta-atoms are employed to further improve the impedance matching of the patch in the operating frequency bands. Then, by arranging unit As and unit Bs into an interleaved form to wrap onto the metallic cylinder as

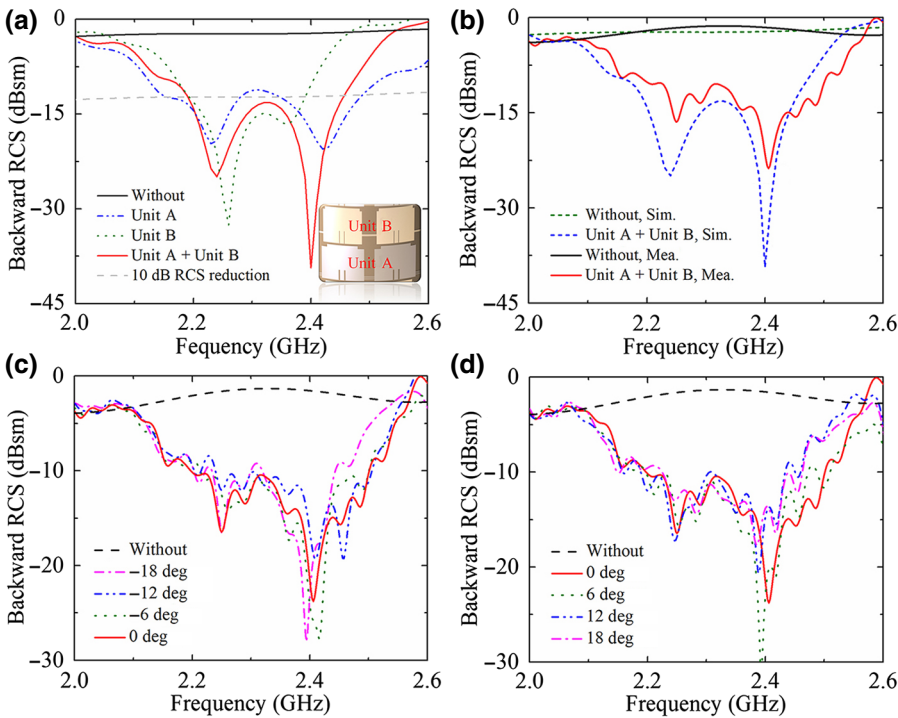


FIG. 7. (a) Backward RCS for the metallic cylinder covered with cloak composed of unit As, unit Bs, or both of them. Inset shows the enlarged view of unit As and unit Bs. (b) Simulated and measured backward RCS results of the cylindrical object with and without the cloak composed of unit As and unit Bs, and the measured results for different self-rotational angles (c) from -18° to 0° , and (d) from 0° to 18° .

depicted in S8(c) of the Supplemental Material [47], we finally configure a conformal cloak with its performance of backward scattering plotted with the red line in Fig. 7(a). It is clear that the operating band for backward-scattering suppression can be improved to a continuous band from 2.0 to 2.5 GHz by combining the two types of meta-atoms. The fractional bandwidth with respect to the center frequency of 2.32 GHz exceeds 11.64%, which is competitive compared to other passive single-layered cloaking strategies with ultrathin profile [2,5,40,41].

The prototype of the cloak combining two kinds of elements is shown in Fig. S10 of Supplemental Material [47]. The measured and simulated results of monostatic RCS of the metallic cylinder with and without conformal metasurface are shown in Fig. 7(b). It can be seen that the cloak can efficiently suppress the backward scattering of the metallic cylinder across the band from 2.0 to 2.57 GHz, and the measured 10 dB bandwidth can reach 2.234–2.496 GHz, approximately 11.10% fractional bandwidth with respect to the center frequency of 2.36 GHz. The minor discrepancies between the simulated and measured results are attributed to imperfect fabrication, assembly and experimental measurements, for example, the little distort flatness of the conformal cloak when it is wrapped onto the cylinder. Compared with the metasurface consisting of a single kind of meta-atom [Fig. 6(a)], this scheme can efficiently increase the bandwidth of 10-dB reduction of monostatic RCS by about 44.72%.

We finally test the rotational stability of the proposed cloak. The size of meta-atoms leads to a periodicity in term of azimuth angle of 36° when the cloak is wrapped onto the metallic cylinder, so the backward-scattering results are illustrated within the rotational angle of $\pm 18^\circ$. The results are shown in Figs. 7(c) and 7(d), where the bandwidth gradually decreases as the increase of self-rotational angle (φ), but the fractional bandwidth over 8.4% can be obtained, regardless of the change of φ . The above results confirm that the proposed cloak has good robustness to the self-rotational angel.

V. CONCLUSIONS

In summary, we propose a composite strategy by combining the mechanisms of Mie-scattering theory and microwave network to design the metasurface cloak for backward-scattering reduction. As an example, we experimentally show that a conformal metasurface with ultrathin profile (0.0156 wavelength) can provide a fractional bandwidth of around 7.67% of efficient monostatic RCS suppression for cylinder target with wavelength-scale size. Moreover, by combining meta-atoms with different geometrical dimensions, we extend the working bandwidth of the metasurface cloak for monostatic RCS reduction. Experimental measurements show that an improved bandwidth of 11.10% can be achieved. It should be noted that

the proposed composite strategy is not limited to broaden the operating bandwidth herein, other functionalities, e.g., dual-band cloaks, can also be realized thanks to the independent design of Mie-scattering theory and microwave transmission network. In addition, the design methodology can be readily scaled to other frequency bands such as, millimeter-wave, and terahertz band, etc. We also envision a tunability of the cloak by incorporating active components, e.g., graphene or diodes. With the advantages of simple design and improved bandwidth, the proposal may find potential uses in many engineering applications such as antenna isolation, camouflaging, etc.

ACKNOWLEDGMENTS

This work is supported by National Key Research and Development Program of China (Grant No. 2017YFA0700201); National Natural Science Foundation of China (NSFC) (61671231, 61801207, 61731010, and 61571218). This work is partially supported by the Priority Academic Program Development of Jiangsu Higher Education Institutions (PAPD), the Fundamental Research Funds for the Central Universities and Jiangsu Provincial Key Laboratory of Advanced Manipulating Technique of Electromagnetic Wave, and the Program B for Outstanding PhD Candidate of Nanjing University.

- [1] P. Y. Chen, J. Soric, and A. Alù, Invisibility and cloaking based on scattering cancellation, *Adv. Mater* **24**, OP281 (2012).
- [2] J. Wang, S. Qu, Z. Xu, H. Ma, J. Zhang, Y. Li, and X. Wang, Super-thin cloaks based on microwave networks, *IEEE Trans. Antennas Propag* **61**, 748 (2013).
- [3] J. C. Soric, A. Monti, A. Toscano, F. Bilotti, and A. Alù, Dual-polarized reduction of dipole antenna blockage using mantle cloaks, *IEEE Trans. Antennas Propag* **63**, 4827 (2015).
- [4] R. Fleury, D. Sounas, and A. Alù, An invisible acoustic sensor based on parity-time symmetry, *Nat. Commun* **6**, 5905 (2015).
- [5] A. Rajput and K. V. Srivastava, Dual-band cloak using microstrip patch with embedded U-shaped slot, *IEEE Antennas Wireless Propag. Lett.* **16**, 2848 (2017).
- [6] F. Aieta, P. Genevet, N. Yu, M. A. Kats, Z. Gaburro, and F. Capasso, Out-of-plane reflection and refraction of light by anisotropic optical antenna metasurfaces with phase discontinuities, *Nano Lett.* **12**, 1702 (2012).
- [7] A. V. Kildishev, A. Boltasseva, and V. M. Shalaev, Planar photonics with metasurfaces, *Science* **339**, 1232009 (2013).
- [8] P. Genevet, F. Capasso, F. Aieta, M. Khorasaninejad, and R. Devlin, Recent advances in planar optics: From plasmonic to dielectric metasurfaces, *Optica* **4**, 139 (2017).
- [9] K. Chen, Y. Feng, F. Monticone, J. Zhao, B. Zhu, T. Jiang, L. Zhang, Y. Kim, X. Ding, S. Zhang, A. Alù, and C.-W. Qiu, A reconfigurable active Huygens' metalens, *Adv. Mater* **29**, 1606422 (2017).

- [10] B. Sima, K. Chen, X. Luo, J. Zhao, and Y. Feng, Combining Frequency-Selective Scattering and Specular Reflection Through Phase-Dispersion Tailoring of a Metasurface, *Phys. Rev. Appl.* **10**, 064043 (2018).
- [11] S. Liu, T. J. Cui, A. Noor, Z. Tao, H. C. Zhang, G. D. Bai, Y. Yang, and X. Y. Zhou, Negative reflection and negative surface wave conversion from obliquely incident electromagnetic waves, *Light: Sci. Appl.* **7**, 18008 (2018).
- [12] G. Ding, K. Chen, X. Luo, J. Zhao, T. Jiang, and Y. Feng, Dual-Helicity Decoupled Coding Metasurface for Independent Spin-to-orbital Angular Momentum Conversion, *Phys. Rev. Appl.* **11**, 044043 (2019).
- [13] S. Liu, H. X. Xu, H. C. Zhang, and T. J. Cui, Tunable ultrathin mantle cloak via varactor-diode-loaded metasurface, *Opt. Express* **22**, 13403 (2014).
- [14] J. Wang, S. Qu, J. Zhang, H. Chen, H. Ma, and Z. Xu, Design of super-thin cloaks with arbitrary shapes using interconnected patches, *IEEE Trans. Antennas Propag* **63**, 384 (2015).
- [15] Z. H. Jiang, P. E. Sieber, L. Kang, and D. H. Werner, Restoring intrinsic properties of electromagnetic radiators using ultralightweight integrated metasurface cloaks, *Adv. Funct. Mater* **25**, 4708 (2015).
- [16] Y. Huang, Y. Feng, and T. Jiang, Electromagnetic cloaking by layered structure of homogeneous isotropic materials, *Opt. Express* **15**, 11133 (2007).
- [17] T. V. Teperik, S. N. Burokur, A. de Lustrac, G. Sabanowski, and G.-P. Piau, Experimental validation of an ultrathin metasurface cloak for hiding a metallic obstacle from an antenna radiation at low frequencies, *Appl. Phys. Lett.* **111**, 054105 (2017).
- [18] J. Yang, C. Huang, X. Wu, B. Sun, and X. Luo, Dual-wavelength carpet cloak using ultrathin metasurface, *Adv. Opt. Mater* **6**, 1800073 (2018).
- [19] Y. Kim, T. Deng, W. X. Jiang, T. J. Cui, Y. Lee, and C.-W. Qiu, Robust Control of a Multifrequency Metamaterial Cloak Featuring Intrinsic Harmonic Selection, *Phys. Rev. Appl.* **10**, 044027 (2018).
- [20] P. Yuste, J. M. Rius, J. Romeu, S. Blanch, A. Heldring, and E. Ubeda, A microwave invisibility cloak: The design, simulation, and measurement of a simple and effective frequency-selective surface-based mantle cloak, *IEEE Antennas Propag. Mag* **60**, 49 (2018).
- [21] W. Jiang, Y. Ma, and S. He, Static Magnetic Cloak Without a Superconductor, *Phys. Rev. Appl.* **9**, 054041 (2018).
- [22] H. Chu, Q. Li, B. Liu, J. Luo, S. Sun, Z. H. Hang, L. Zhou, and Y. Lai, A hybrid invisibility cloak based on integration of transparent metasurfaces and zero-index materials, *Light: Sci. Appl.* **7**, 50 (2018).
- [23] J. B. Pendry, D. Schurig, and D. R. Smith, Controlling electromagnetic fields, *Science* **312**, 1780 (2006).
- [24] D. Schurig, J. J. Mock, B. J. Justice, S. A. Cummer, J. B. Pendry, A. F. Starr, and D. R. Smith, Metamaterial electromagnetic cloak at microwave frequencies, *Science* **314**, 977 (2006).
- [25] U. Leonhardt, Optical conformal mapping, *Science* **312**, 1777 (2006).
- [26] C. W. Qiu, L. Hu, X. Xu, and Y. Feng, Spherical cloaking with homogeneous isotropic multilayered structures, *Phys. Rev. E* **79**, 047602 (2009).
- [27] B. Zhang, Y. Luo, X. Liu, and G. Barbastathis, Macroscopic Invisibility Cloak for Visible Light, *Phys. Rev. Lett.* **106**, 033901 (2011).
- [28] X. Chen, Y. Luo, J. Zhang, K. Jiang, J. B. Pendry, and S. Zhang, Macroscopic invisibility cloaking of visible light, *Nat. Commun* **2**, 176 (2011).
- [29] X. Zhu, L. Feng, P. Zhang, X. Yin, and X. Zhang, One-way invisible cloak using parity-time symmetric transformation optics, *Opt. Lett.* **38**, 2821 (2013).
- [30] H. Chen and B. Zheng, Broadband polygonal invisibility cloak for visible light, *Sci. Rep.* **2**, 255 (2012).
- [31] H. Chen, B. Zheng, L. Shen, H. Wang, X. Zhang, N. I. Zhe-ludev, and B. Zhang, Ray-optics cloaking devices for large objects in incoherent natural light, *Nat. Commun.* **4**, 2652 (2013).
- [32] M. Gharghi, C. Gladden, T. Zentgraf, Y. Liu, X. Yin, J. Valentine, and X. Zhang, A carpet cloak for visible light, *Nano Lett.* **11**, 2825 (2011).
- [33] S. Tretyakov, P. Alitalo, O. Luukkonen, and C. Simovski, Broadband Electromagnetic Cloaking of Long Cylindrical Objects, *Phys. Rev. Lett.* **103**, 103905 (2009).
- [34] P. Alitalo, F. Bongard, J. F. Zürcher, J. Mosig, and S. Tretyakov, Experimental verification of broadband cloaking using a volumetric cloak composed of periodically stacked cylindrical transmission-line networks, *Appl. Phys. Lett.* **94**, 014103 (2009).
- [35] A. Alù and N. Engheta, Achieving transparency with plasmonic and metamaterial coatings, *Phys. Rev. E* **72**, 016623 (2005).
- [36] B. Edwards, A. Alù, M. G. Silveirinha, and N. Engheta, Experimental Verification of Plasmonic Cloaking at Microwave Frequencies with Metamaterials, *Phys. Rev. Lett.* **103**, 153901 (2009).
- [37] A. Alù, Mantle cloak: Invisibility induced by a surface, *Phys. Rev. B* **80**, 245115 (2009).
- [38] J. C. Soric, A. Monti, A. Toscano, F. Bilotti, and A. Alù, Multiband and wideband bilayer mantle cloaks, *IEEE Trans. Antennas Propag* **63**, 3235 (2015).
- [39] J. C. Soric, P. Y. Chen, A. Kerkhoff, D. Rainwater, K. Melin, and A. Alù, Demonstration of an ultralow profile cloak for scattering suppression of a finite-length rod in free space, *New J. Phys.* **15**, 033037 (2013).
- [40] S. Liu, H. C. Zhang, H.-X. Xu, and T. J. Cui, Nonideal ultrathin mantle cloak for electrically large conducting cylinders, *J. Opt. Soc. Am. A* **31**, 2075 (2014).
- [41] H. Younesiraad, M. Bemani, and S. Nikmehr, Scattering suppression and cloak for electrically large objects using cylindrical metasurface based on monolayer and multilayer mantle cloak approach, *IET Microw. Antennas Propag* **13**, 278 (2019).
- [42] J. Valentine, J. Li, T. Zentgraf, G. Bartal, and X. Zhang, An optical cloak made of dielectrics, *Nat. Mater* **8**, 568 (2009).
- [43] R. Mittra, *Computational Electromagnetics* (Springer-Verlag, New York, 2016).
- [44] C. Argyropoulos, E. Kallos, Y. Zhao, and Y. Hao, Manipulating the loss in electromagnetic cloaks for perfect wave absorption, *Opt. Express* **17**, 8467 (2009).
- [45] H. Hashemi, B. Zhang, J. D. Joannopoulos, and S. G. Johnson, Delay-Bandwidth and Delay-Loss Limitations for

- Cloaking of Large Objects, *Phys. Rev. Lett.* **104**, 253903 (2010).
- [46] F. Monticone and A. Alù, Invisibility exposed: Physical bounds on passive cloaking, *Optica* **3**, 718 (2016).
- [47] See the Supplemental Material at <http://link.aps.org/supplemental/10.1103/PhysRevApplied.12.064027> for more discussions on the optimum surface reactance, equivalent transmission line model for meta-atom, electric field, and power flow distribution comparisons, the effect of dielectric loss and R_s on the backward RCS reduction, additional results for the optimized planar meta-atom, measurement setup for the designed metasurface cloak, bandwidth enhancement by combining unit As and unit Bs, additional results for the unit A and unit B and fabrication prototype of the cloak combining unit As and unit Bs.
- [48] Y. R. Padooru, A. B. Yakovlev, P. Y. Chen, and A. Alù, Analytical modeling of conformal mantle cloaks for cylindrical objects using sub-wavelength printed and slotted arrays, *J. Appl. Phys.* **112**, 034907 (2012).
- [49] C. Pfeiffer and A. Grbic, Metamaterial Huygens' Surfaces: Tailoring Wave Fronts with Reflectionless Sheets, *Phys. Rev. Lett.* **110**, 197401 (2013).
- [50] A. Díaz-Rubio, V. S. Asadchy, A. Elsakka, and S. A. Tretyakov, From the generalized reflection law to the realization of perfect anomalous reflectors, *Sci. Adv.* **3**, e1602714 (2017).
- [51] R. S. Schofield, J. C. Soric, D. Rainwater, A. Kerkhoff, and A. Alù, Scattering suppression and wideband tunability of a flexible mantle cloak for finite-length conducting rods, *New J. Phys.* **16**, 063063 (2014).